Molecular dynamics of carbon nanotubule proximal probe tip-surface contacts

Ajay Garg and Susan B. Sinnott*
Department of Chemical and Materials Engineering, The University of Kentucky, Lexington, Kentucky 40506-0046
(Received 18 February 1999; revised manuscript received 21 May 1999)

The mechanisms by which carbon nanotubule (CNT) proximal probe tips deform during the indentation of surfaces are explored using classical molecular-dynamics simulations. The forces acting on the atoms in the simulations are calculated using the Brenner empirical bond-order potential for hydrocarbons. The results show that open and capped single-walled CNT tips indented against hydrogen-terminated diamond and graphene surfaces buckle and slip to relieve the applied stress. The study also examines the indentation of capped multiwalled tubules against these surfaces to investigate the effect of multiple shells on the deformation process. It is found that while shell-shell interactions have little effect on the deformation mechanisms, the multiwalled tubule is significantly stiffer than comparably sized single-walled tubules. No bond formation between the shells is predicted as a result of deformation. Finally, a small CNT rope is indented against diamond and graphene to assess the effect of intertubule interactions on deformation. The simulations reveal how the deformation of the rope leads to the distortion of its end and allow for the determination of the effect of shear stress within the bundle on the buckling force of the rope. [S0163-1829(99)03643-7]

INTRODUCTION

Over the last few years, there have been many studies of the mechanical properties of carbon nanotubules (CNT's), particularly to determine the maximum strain they can undergo and their maximum mechanical load-bearing capacity. These mechanical properties have been investigated experimentally[1–7] and by various computational methods, including empirical force constant models,[8–10] tight-binding approximation methods,[11–14] first-principles total energy methods,[15,16] and empirical potential molecular-dynamics simulations.[17–24] These calculations and experimental measurements have determined that CNT's possess high-Young's moduli in the range of 1–5 TPa. In addition, CNT's can be insulating, semiconducting, or metallic depending on their helical structure.[25–27]

These properties strongly suggest the application of CNT's in proximal probe microscopy. Dai *et al.*[28] first used metallic (10,10) CNT's as tips for a scanning force microscope to image nanometer and micrometer-scale structures. Their CNT was about 2 μm long with a radius of 0.68 nm and was shown to provide increased resolution over traditional Pt/W scanning tunneling microscopy tips that are typically 1–100 nm in size at the apex. However, despite the sharpness of the tip, atomic-scale resolution was difficult to achieve due to the thermal vibrations that long CNT's undergo at room temperature.[29] Subsequently, CNT proximal probe tips were chemically functionalized to allow for chemical or biological imaging of a sample.[30] They have also recently been used to make detailed nanometer-scale silicon-oxide patterns on silicon surfaces by biasing the CNT negatively with respect to the surface and using the CNT for contact mode atomic force microscopy lithography.[31]

In this work, shortened tips that do not undergo significant thermal vibration are studied. Experimentally, these shortened nanotubules could be obtained using the cutting technique discussed in Ref. 30 or grown directly on the end of a silicon tip, as recently done by Lieber and coworkers.[32] The objective of this work is to study CNT tip-surface interactions during nanoindentation similar to that reported in Ref. 31. This is accomplished through a systematic study of the variation of these interactions with changes in surface properties, tubule type, and tubule length. Specifically, the indentation of open, single-walled tubules, capped, multiwalled tubules, and a small, capped, CNT rope (bundle) with diamond and graphene are examined and the results reported below. Indentation results for capped, single-walled tubules are reported in detail in a recent publication.[33]

COMPUTATIONAL TECHNIQUES

Classical molecular-dynamics method are used where Newton's equations of motion are solved numerically for a set of atoms or molecules interacting via a given potential energy (ϑ). The potential energy of the system is determined using the well-known reactive empirical bond-order hydrocarbon potential formulated by Brenner[34,35] for intermolecular interaction, which unlike force-field methods allows for bond formation and breaking to occur. This potential was originally developed[34] to study diamond chemical vapor deposition but has since found application in modeling numerous other hydrocarbon systems. A second-generation version of this potential was subsequently developed[35] that contains improved analytic functions for intramolecular interactions and an expanded fitting database that includes small hydrocarbon molecules, radicals, graphite, and diamond. The Brenner potential has been successfully used to simulate numerous processes including the deformation of CNT's,[17–24] the nanometer-scale indentation of diamond surfaces[36,37] and amorphous carbon thin films[36,38] with diamond tips, and the formation of fullerenes from graphitic ribbons.[39]

Because the atoms are treated as hard spheres, forces from electronic effects like orbital resonance and symmetry are neglected. In addition, since this potential is comparatively short ranged, long-ranged forces are not included. Therefore,

van der Waals energies are added to the covalent terms using Lennard-Jones (LJ) potentials. The combined mathematical expression to calculate the potential energy of a system of N atoms is:

$$\vartheta(r_{ij}) = \sum_{i}^{N} \sum_{j<i}^{N} [V_r(r_{ij}) - B_{ij} V_a(r_{ij}) + V_{vdW}(r_{ij})], \quad (1)$$

where r_{ij} is the distance between atoms i and j, V_r and V_a are pair-additive repulsive and attractive interactions, respectively, and B_{ij} is a many-body coupling between the bond from atom i to atom j and local environment of atom i. V_{vdW} is the energy due to the van der Waals interactions. The terms V_r, V_a, and B_{ij} are short-range whereas V_{vdW} accounts for all the long-range interactions and is nonzero only after the short-range covalent potential goes to zero.

Two different LJ potentials are used for V_{vdW} in these simulations to remove any influence of the specific LJ potential on the results. The first was formulated for the study of liquid *n*-butane near its boiling point[40] while the second was formulated for generic hydrocarbon systems.[41] However, no significant differences in results are found using these two different LJ formulations and so the results are reported without specifying LJ potential.

The surfaces considered in the study are hydrogen-terminated diamond (111), C(111):H, and a graphene sheet. The simulations are carried out at 300 K and a time step of 0.15 fs is used. In the case of the single-walled and multiwalled tubule indentations, two different diamond surfaces are used in the simulations. The first consists of 20 layers of carbon, with each layer containing 370 atoms. The top and bottom layers are hydrogen terminated. The second surface consists of six layers of carbon that again had 370 atoms/layer.

Open single-walled (10,10) nanotubules with lengths of 5.0 and 8.1 nm are examined. In the multiwalled case, an 8.1 nm-long capped, two-shell CNT is used with a (15,15) tubule for the outer shell and a (10,10) tubule for the inner shell. To mimic the rigid cantilever attached to the tip used in the experiments, the top 100 atoms of the (10,10) CNT [150 atoms of the (15,15) CNT] farthest from the surface are held rigid. This follows the example of Landman *et al.*[42] that has been subsequently used in several other indentation simulations.[33,36,37] To hold the diamond surfaces in space, 1480 atoms at the base of the diamond (farthest from the top) are also held rigid throughout the simulation. Moving toward the middle of the system, a Langevin thermostat is applied to the next 200 atoms of the nanotubule and two layers of the substrate. The remaining atoms (active atoms) of both the nanotubule and the substrate evolve according to Newton's equations of motion with no constraints.

When the CNT tip indents the graphene sheet, the arrangements of active, Langevin, and rigid atoms for the tubule are identical to those used for the diamond surface indentation. The graphene sheet is circular with a diameter of about 8 nm and the outermost atoms are held rigid. Moving inwards, a Langevin thermostat is applied to the next 0.7 nm of thickness around the circumference. The remaining atoms in the sheet are active.

The indentation process proceeds as follows. The top is positioned about 0.2 nm above the surface and moves towards the surface in increments of 0.005 nm. Each displacement step is followed by 400 relaxation steps in order to dampen out the effects of the preceding displacement step. It should be pointed out that the indentation proceeds at a faster rate than is seen experimentally. This is because of computational limitations that currently prohibit the simulation of nanoindentation at experimental rates. Despite these limitations, much insight has been possible from nanonindentation simulations[33,36,37,42] such as are used in this study.

When the tip displacement towards the surface becomes larger than the initial spacing between the tip and the surface, the tip is compressed against the surface. After indentation the tubules are pulled back in a similar fashion with negative displacement. The force on the 100 fixed atoms of the CNT tip that are displaced is calculated as follows:

$$F_i = -[\delta \vartheta(r^N)]/\delta r_i \quad (2)$$

$$F_{\text{total}} = \sum_{i}^{M} F_i, \quad (3)$$

where $\vartheta(r^N)$ is the potential energy of atom i due to the surrounding N atoms, r_i is the atomic coordinate of atom i, and F_i is the force on atom i. The atomic forces are calculated at each of the 400 relaxation steps following each displacement and then averaged over the last 100 steps. Force displacement curves are then plotted using these averaged values against displacement steps. Additional averaging is performed on the resulting force curves to filter out the noise from thermal vibrations. These conditions are similar to those previously used to model the indentation of C(111):H with capped single-walled CNT's (Ref. 33) and with a square-pyramidal, hydrogen-terminated diamond asperity tip.[36]

The small CNT rope or bundle is constructed by placing four capped (10,10) nanotubules with length 8.1 nm in a rhombus pitch. The length of the pitch is 0.35 nm as observed by many experimental researchers.[43] It is indented on a wider C(111):H surface composed of six layers where each layer contains 533 atoms. The top 100 atoms of each of the carbon nanotubule (farthest from the surface), i.e., 400 atoms of the bundle and the 1066 atoms at the base of the diamond (farthest from the tip) are held rigid throughout the simulations. A Langevin thermostat is applied to the next 800 atoms of the bundle (200 atoms of each nanotubule) and two layers of the substrate. The remaining atoms are active. When the CNT bundle tip indents the graphene sheet, the arrangements of active, Langevin, and rigid atoms for the tubule are the same as indicated above for the single-walled and multiwalled CNT's.

RESULTS AND DISCUSSION

Single aanotubule proximal probe tips

The first series of simulations examined the indentation of the 20-layer C(111):H surface with open, hydrogen-terminated (10,10) nanotubes of various lengths. This is motivated by the fact that purification methods usually result in opened nanotubes.[44] As the tips push against the surface, kinks or buckles develop in the body of the tubules to relieve stress in a manner that is very similar to what was seen with

capped single-walled tubules.[33] The force on the tips increases rapidly because of repulsion between the hydrogen atoms on the end of the tip and on the surface. The force curves have average slopes of around 120 nN/nm, an order of magnitude higher than that seen for comparable capped single-walled CNT's indenting this surface.[33] The maximum force felt by both the 5.0 and 8.1 nm-long CNT tips prior to slip is about 82 nN. This is only slightly higher than the value of 80 nN found for the corresponding capped CNT's.[33]

When the tips have been pushed 0.4 nm against the surface, they abruptly slip such that the tubules are sharply bent with the ends pointing up. This is about half the distance that the capped tubules were pushed prior to slip.[33] In general, as the tips increase in length, they are able to press farther against the surface before slipping and bending. Pushing the tubules further after slip cause the bend to move up the length of the CNT as the end pointing up grows longer. The diamond surface does not undergo any deformation whatsoever, justifying the use of the six-layer diamond surface mentioned above in some of the simulations. When the tips are retracted, they return to their original structures in a manner similar to that seen for the capped tubules in Ref. 33 and in agreement with available experimental data.[28,31]

Thus, in the preceding simulations the indentations are elastic on the time scale of the simulation. This is in contrast to the results of simulations of diamond asperity tips indenting C(111):H,[36] where the tips deformed through twist and shear mechanisms up to an indentation depth of about 0.5 nm before bonds within the tips began to break in a brittle fashion. This resulted in adhesion between the tips and the surface not seen in the simulations with the CNT tips on this surface. Hence, the tubules are shown to withstand failure when crashed or pressed against rigid, passivated surfaces due to their flexibility to buckle, bend, and slip to relieve applied stress.

Similar mechanisms to relieve stress are predicted when capped[33] and hydrogen terminated, open CNT tips are indented against the graphene sheet, a surface that is compliant and easily deformed. As the CNT tips indent the graphene, the sheet deforms forming a well-like structure. The tips are pushed against the surface for 1.5 nm before the tips buckle and slip in a manner very similar to what was seen for indentation on the C(111):H surface. On retraction, both the CNT tips and the graphene sheet return to their original configurations. The combined flexibility of the CNT tips and the graphene leads to a smaller average slope of 10 nN/nm for the force curve. The buckling force is about 100 nN for the capped and open tubules, which is larger than comparable buckling forces for either seen in diamond indentation. This is due to the fact that the deformed, well-like graphene sheet prevents the CNT from slipping as readily as with a diamond surface, i.e., it reduces the degrees of freedom available to the tip. Thus, there are fewer differences between open and capped single-walled CNT's indenting graphene than C(111):H.

Next, we extend this study to examine the effects of adding an additional shell to the CNT on the indentation process. This corresponds to changing the proximal probe from a single-walled CNT to a double-shelled, multiwalled CNT. When this tip indents the C(111):H surface, it buckles and then slips in a manner that is very similar to the deformation

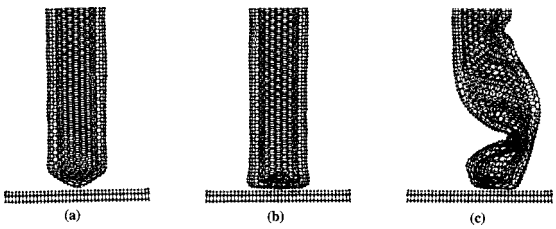

FIG. 1. Snapshots of the indentation of an 8.1 nm-long, capped multiwalled tubule on the C(111):H surface. The tubule consists of a (10,10) tube inside a (15,15) tube. (a) Starting configuration, (b) inversion of the inner and outer caps, and (c) slip after buckling twice.

of the single-walled CNT's and as illustrated in Fig. 1. the kinks and buckles develop in both the inner and outer tubules at the same time and both tubules slip together. When the tubule is pulled back no chemical bonds had broken or new bonds formed between the tubule shells.

It has been shown experimentally[2,6] and theoretically[9] that, in general, multiwalled tubules are stiffer than single-walled tubules and the stiffness increases as the number of shells increase. This result is also predicted in these simulations, as shown in Fig. 2, where the force curves obtained for the indentation of a single, capped (15,15) tubule and the multiwalled tubule on C(111):H are shown for comparison. The buckling force for the multiwalled tubule (normalized by the number of atoms used to calculate the force) of 101 nN/100 atoms is larger than the buckling force of a single-walled (15,15) tubule of 94 nN/100 atoms. When the multiwalled tubule indents the graphene sheet, inversion of both the inner and outer caps, buckling, and slip are also seen. The buckling force for the graphene indentation of about 106 nN/100 atoms is slightly larger than the buckling force calculated for the C(111):H indentation.

Hence, these simulations predict that the van der Waals interactions between two shells in a multiwalled tubule do not affect the qualitative deformation behavior but do increase the buckling force of the tip on indentation of compliant or stiff surfaces. They also lessen the effect of the flexibility of the surface on the buckling force of the tube. Finally, the simulations do not predict bond formation between the shells on deformation.

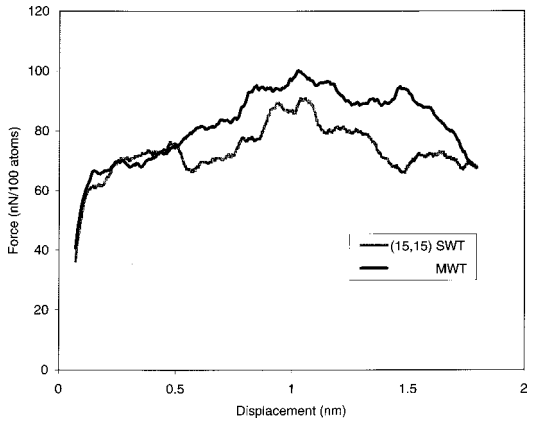

FIG. 2. Force curve from the indentation of a capped multiwalled tubule that consists of a (10,10) tube inside a (15,15) tube, and a single-walled (15,15) tube on the C(111):H surface.

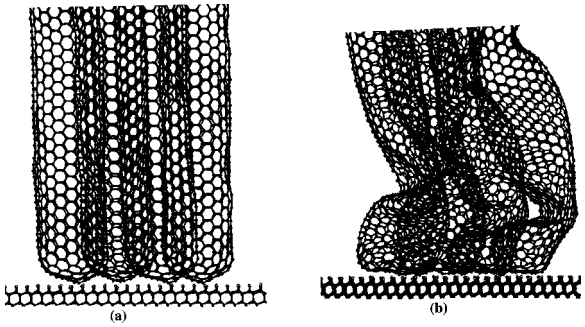

FIG. 3. Snapshots from the indentation of a rope of four capped (10,10) tubules against the C(111):H surface. (a) is the starting configuration and (b) is after buckling.

Nanotubule bundle proximal probe tips

Numerous scanning electron microscopy images of CNT formation has shown them to frequently grow in bundles.[45] Hence, this study is further extended to CNT bundle interaction with these surfaces to see how van der Waals interactions between the tubules affect the indentation process.

In the first series of simulations, the rope is indented against the C(111):H surface. As the indentation proceeds, the CNT rope compresses against the surface and then deforms as shown in Fig. 3. The simulations predict the same deformation mechanisms discussed above of cap inversion, multibuckle formation, and finally slipping. The maximum buckling force felt by the CNT rope indenting a C(111):H surface is about 340 nN. This corresponds to a maximum buckling force of 85 nN/tubule in the bundle, a value that is higher than the individual, capped, single-wall CNT buckling force of 80 nN found in Ref. 33. This increase is caused by the van der Waals interactions between the CNT's in the rope that restrict the degrees of freedom of each CNT within the bundle to slip. This is analogous to what was seen for the single CNT's indenting the graphene sheet. When the tip is withdrawn, there are only minor distortions of the bundle.

Next, the tubule bundle is indented against the graphene sheet. During compression, the caps of all the nanotubules are flattened. This is followed by a single buckle forming very close to the tip end for three of the tubules and two buckles forming for one of the tubules. Finally, slip on the graphene surface is seen with one of the tubules slipping significantly more than the others as shown in Fig. 4. The maximum buckling force felt by the CNT bundle is about 305 nN. This results in a maximum force per nanotubule of 76 nN, i.e., 24 nN/tubule *lower* than the force experienced by a single CNT tip[33] during indentation of graphene sheet. This is in contrast to what is seen for single-walled CNT's that have *higher* buckling forces on the more compliant graphene sheet. On pull up, the bundle is distorted with the tubule ends father apart than at the start of the simulation.

This degradation of the maximum force in the bundle tip is because the tubule ends within the bundle are pushed close to one another by the deformation of the graphene sheet into a well-like structure. This generates outward shear forces within the bundle that cause the tubules to slip more rapidly, thus lowering the maximum buckling force of the CNT bundle tip.

A third set of simulations is performed to more fully understand the interactions within the CNT bundle itself. The two ends of the bundle are kept rigid and one of them is moved towards the other in a manner similar to that employed in the indentation processes. The maximum buckling force predicted for this ''free-space'' compression is about 450 nN, significantly higher than the buckling force of the rope on either the diamond or the graphene surfaces. This is because of the bundle's inability to relieve stress through mechanisms other than buckling, such as slip. The maximum buckling force during free space compression per CNT in the bundle is 112 nN, which is 8 nN/tubule lower than that for a single CNT undergoing free-space compression.[33] This difference is again due to the shear stresses generated by the repulsive intertubule interactions during compression.

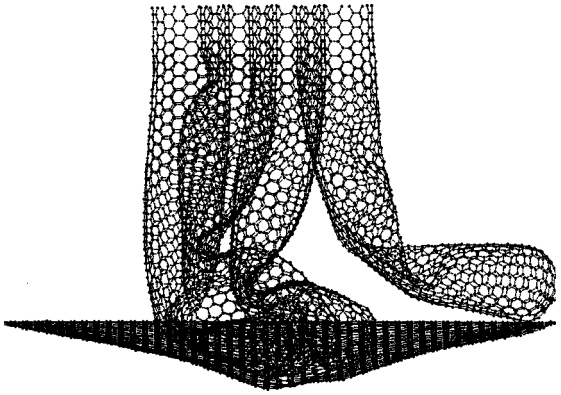

FIG. 4. Snapshot from the indentation of a rope of four capped (10,10) tubules against a graphene sheet during the pull-back phase. The tubule on the far right buckled twice on indentation while the others buckled only once. The figure shows how the rope end is distorted as a result of the indentation.

Figure 5 shows a comparison of the buckling force curves for the CNT bundle during free-space compression, indentation of the C(111):H surface, and indentation of the graphene sheet. The figure clearly shows that the maximum buckling force of a CNT bundle is *not* a simple summation of the forces on a corresponding number of individual CNT's indenting the same surface. Furthermore, the maximum buckling force of the bundle depends on the rigidity of the indented surface and decreases with a decrease in surface rigidity. This is in contrast to single CNT indentation where the maximum buckling force of the CNT is observed to increase with a decrease in surface rigidity.

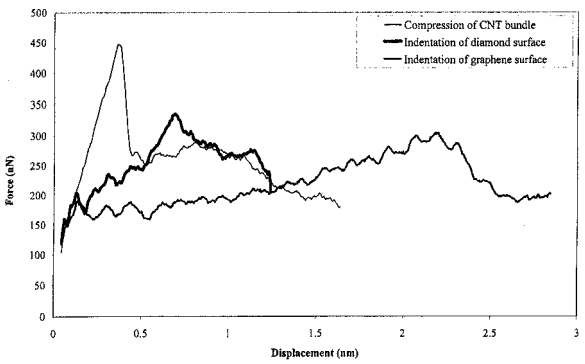

FIG. 5. Force curves for the nanotube rope during compression in free space, against a hydrogen-terminated, diamond (111) surface and against a graphite sheet.

CONCLUSIONS

Molecular-dynamics simulations using a many-body empirical hydrocarbon potential coupled to a long-range Lennard-Jones potential have been carried out to investigate the indentation of CNT-based tips against various surfaces. The results indicate that short, single-walled nanotubules do not plastically deform during tip crashes on inert surfaces like diamond asperity tips. Instead, they elastically deform, buckle, and slip, mechanisms that will have to be taken into account when CNT tips are used in proximal probe microscopes. Furthermore, the maximum buckling force shows a strong dependence on the type of the surface used, increasing with decreases in the rigidity of the surface. This is because of a decrease in the degrees of freedom at the tip end that restricted its freedom to slip. There is also a significant difference in predicted buckling force and speed of buckling and slip when the tubule is hydrogen-terminated versus capped during the indentation of rigid, hydrogen-terminated diamond. There is much less difference on indenting compliant graphene.

Two-shell multiwalled tubules are predicted to deform in a similar manner to single-walled tubules but with significantly higher buckling forces. No bond formation is predicted between the tubule shells despite the deformation of the tubule. The simulations also predict that single-walled tubules in a bundle undergo similar stress relieving contortions. However, intrabundle interactions due to shear forces, absent in single CNT indentation, play a critical role in determining the maximum buckling force of the CNT rope tip. The maximum buckling force behavior of these bundle tips is in direct contrast to that of individual CNT tips and cannot be determined using a simple summation of the forces of a comparable number of tubules.

ACKNOWLEDGMENTS

The authors acknowledge many helpful discussions with Dr. Jie Han (NASA-Ames) and Professor Peter Eklund (University of Kentucky). We also gratefully acknowledge the support of the NASA Ames Research Center (Grant No. NAG 2-1121) and a National Science Foundation MRSEC (Grant No. DMR-9809686).

*Author to whom correspondence should be addressed.

[1] P. M. Ajayan, O. Stephan, C. Colliex, and D. Trauth, Science **265**, 1212 (1994).
[2] M. M. J. Treacy, T. W. Ebbesen, and J. M. Gibson, Nature **381**, 678 (1996).
[3] W. H. Knechtel, G. S. Dusberg, W. J. Blau, E. Hernandez, and A. Rubio, Appl. Phys. Lett. **73**, 1961 (1998).
[4] A. Krishnan, E. Dujardin, T. W. Ebbesen, P. N. Yianilos, and M. M. J. Treacy, Phys. Rev. B **58**, 14 013 (1998).
[5] O. Lourie, D. M. Cox, and H. D. Wagner, Phys. Rev. Lett. **81**, 1638 (1998).
[6] E. W. Wong, P. E. Sheehan, and C. M. Lieber, Science **277**, 1971 (1997).
[7] N. G. Chopra and A. Zettl, Solid State Commun. **105**, 297 (1998).
[8] N. Yao and V. Lordi, J. Appl. Phys. **84**, 1939 (1998).
[9] T. Hertel, R. E. Walkup, and P. Avouris, Phys. Rev. B **58**, 13 870 (1998).
[10] N. Yao and V. Lordi, Phys. Rev. B **58**, 12 649 (1998).
[11] J. M. Molina, S. S. Savinsky, and N. V. Khokhriakove, J. Chem. Phys. **104**, 4652 (1996).
[12] J. P. Lu, Phys. Rev. Lett. **79**, 1297 (1997).
[13] E. Hernandez, C. Goze, P. Bernier, and A. Rubio, Phys. Rev. Lett. **80**, 4502 (1998).
[14] P. Zhang, P. E. Lammert, and V. H. Crespi, Phys. Rev. Lett. **81**, 5346 (1998).
[15] D. H. Robertson, D. W. Brenner, and J. W. Mintmire, Phys. Rev. B **45**, 12 592 (1992).
[16] A. Maiti, C. J. Brabec, C. M. Roland, and J. Bernholc, Phys. Rev. Lett. **73**, 2468 (1994).
[17] S. B. Sinnott, O. A. Shenderova, C. T. White, and D. W. Brenner, Carbon **36**, 1 (1998).
[18] B. I. Yakobson, C. J. Brabec, and J. Bernholc, Phys. Rev. Lett. **76**, 2511 (1996).
[19] C. F. Cornwell and L. T. Wille, Solid State Commun. **101**, 555 (1997).
[20] J. A. Harrison, S. J. Stuart, D. H. Robertson, and C. T. White, J. Phys. Chem. B **101**, 9682 (1997).
[21] C. F. Cornwell and L. T. Wille, J. Chem. Phys. **109**, 763 (1998).
[22] M. B. Nardelli, B. I. Yakobson, and J. Bernholc, Phys. Rev. Lett. **81**, 4656 (1998).
[23] A. Garg and S. B. Sinnott, Chem. Phys. Lett. **295**, 273 (1998).
[24] B. I. Yakobson, M. P. Campbell, C. J. Brabec, and J. Bernholc, Comput. Mater. Sci. **8**, 341 (1997).
[25] S. J. Tans, M. H. Devoret, H. Dai, A. Thess, R. E. Smalley, L. J. Geerligs, and C. Dekker, Nature (London) **386**, 474 (1997).
[26] H. Dai, E. W. Wong, and C. M. Lieber, Science **272**, 523 (1996).
[27] J. W. G. Wildoer, L. C. Venema, A. G. Rinzler, R. E. Smalley, and C. Dekker, Nature (London) **391**, 59 (1998).
[28] H. Dai, J. H. Hafner, A. G. Rinzler, D. T. Colbert, and R. E. Smalley, Nature (London) **384**, 147 (1996).
[29] J. A. Harrison, S. J. Stuart, D. H. Robertson, and C. T. White (unpublished).
[30] S. S. Wong, E. Joselevich, A. T. Woolley, C. L. Cheung, and C. M. Lieber, Nature (London) **394**, 52 (1998); S. S. Wong, A. T. Woolley, T. W. Odom, J.-L. Huang, P. Kim, D. V. Vezenov, and C. M. Lieber, Appl. Phys. Lett. **73**, 3465 (1998).
[31] H. Dai, N. Franklin, and J. Han, Appl. Phys. Lett. **73**, 1508 (1998).
[32] J. H. Hafner, C. L. Cheung, and C. M. Lieber, Nature (London) **398**, 761 (1999).
[33] A. Garg, J. Han, and S. B. Sinnott, Phys. Rev. Lett. **81**, 2260 (1998).
[34] D. W. Brenner, S. B. Sinnott, O. A. Shenderova, and J. A. Harrison (unpublished).
[35] D. W. Brenner, Phys. Rev. B **42**, 9458 (1990).
[36] S. B. Sinnott, R. J. Colton, C. T. White, O. A. Shenderova, D. W. Brenner, and J. A. Harrison, J. Vac. Sci. Technol. A **15**, 936 (1997).
[37] J. A. Harrison, C. T. White, R. J. Colton, and D. W. Brenner, Surf. Sci. **271**, 57 (1992).
[38] J. N. Glosli, M. R. Philpott, and J. Belak, in *Mechanical Behavior of Diamond and Other Forms of Carbon*, edited by M. D. Dory, M. S. Donley, D. Bagley, and J. E. Field, MRS Symposia Proceedings No. 383 (Materials Research Society, Pittsburgh, 1995), p. 431.

[39] D. H. Robertson, D. W. Brenner, and C. T. White, J. Phys. Chem. **96**, 6133 (1992).
[40] J.-P. Ryckaert and A. Bellemans, Chem. Phys. Lett. **30**, 123 (1975).
[41] M. A. Moller, D. J. Tildsley, K. S. Kim, and N. Quirke, J. Chem. Phys. **94**, 8390 (1991).
[42] U. Landman, W. D. Luedtke, N. A. Burnham, and R. J. Colton, Science **248**, 454 (1990).
[43] A. Thess, R. Lee, P. Nikolaev, H. Dai, P. Petit, J. Robert, C. Xu, Y. H. Lee, S. G. Kim, A. G. Rinzler, D. T. Colbert, G. E. Scuseria, D. Tomanek, J. E. Fischer, and R. E. Smalley, Science **273**, 483 (1996).
[44] J. Liu, A. G. Rinzler, H. Dai, J. H. Hafner, R. K. Bradley, P. J. Boul, A. Lu, T. Iverson, K. Shelimov, C. B. Huffman, F. Rodriguez-Macias, Y.-S. Shon, T. R. Lee, D. T. Colbert, and R. E. Smalley, Science **280**, 1253 (1998).
[45] T. W. Ebbesen, Annu. Rev. Mater. Sci. **24**, 235 (1994).